research papers

Structure of the F58W mutant of cytochrome b_5: the mutation leads to multiple conformations and weakens stacking interactions

Li Shan,[a]‡ Jun-Xia Lu,[b] Jian-Hua Gan,[a]§ Yun-Hua Wang,[b] Zhong-Xian Huang[b]* and Zong-Xiang Xia[a]*

[a]State Key Laboratory of Bio-organic and Natural Products Chemistry, Shanghai Institute of Organic Chemistry, Chinese Academy of Sciences, Shanghai 200032, People's Republic of China, and [b]Chemical Biology Laboratory, Department of Chemistry, Fudan University, Shanghai 200433, People's Republic of China

‡ Present address: Department of Biochemistry, Cell and Molecular Biology, University of Tennessee, Knoxville, TN 37997-0840, USA.
§ Present address: Biomolecular Structure Group, NCI-FCRDC, PO Box B, 7th Street, Frederick, MD 21702-1201, USA.

Correspondence e-mail:
zxhuang@fudan.edu.cn, xiazx@mail.sioc.ac.cn

Phe58 of cytochrome b_5 is involved in stacking interactions with heme and the axial ligand His63. To elucidate the contribution of the stacking interactions to protein stability, the crystal structures of the F58Y and F58W mutants were determined at high resolution. The structure of the F58Y mutant is basically the same as that of the wild-type protein. However, the mutation from Phe58 to Trp58 leads to difficulty in growing single crystals and results in a space-group change; the six molecules in the asymmetric unit form two groups that are related by a non-crystallographic twofold axis. The structure of F58W was determined using molecular replacement by making use of the non-crystallographic symmetry. The F58W mutation gives rise to multiple conformations of six side chains, a peptide linking two of the six residues and the extended propionic acid of the heme. The six molecules in the asymmetric unit of the F58W mutant structure are grouped into two types based on their conformations and one of the six molecules exhibits dual conformations. The stacking interactions are weakened owing to the increase/decrease of the angles between the indole ring of Trp58 and the His63/heme rings, which accounts for the lower stability of F58W compared with the wild-type protein.

1. Introduction

Cytochrome b_5 is an electron-transfer protein that is widely distributed in nature. The structure–function relationship of cytochrome b_5 has been studied based on the crystal structures of mutants of cytochrome b_5, the microsomal cytochrome b_5 and the outer mitochondrial membrane cytochrome b_5 (Funk *et al.*, 1990; Rivera *et al.*, 1998; Xue *et al.*, 1999; Wu *et al.*, 2000, 2002; Gan *et al.*, 2002; Wang, Wu *et al.*, 2002; Yao *et al.*, 2002; Cowley *et al.*, 2002; Ren *et al.*, 2004).

The interactions between pairs of aromatic side chains usually make important contributions to protein stability and aromatic amino-acid side chains are commonly observed to interact with the heme cofactors of natural hemoproteins (Burley & Petsko, 1985). These interactions include offset face-to-face π-stacking and edge-to-face T-stacking (Liu *et al.*, 1999; Hunter & Sanders, 1990).

In the cytochrome b_5 structure, Phe58 is an aromatic residue that is located in the heme-binding pocket. The phenyl ring of Phe58 stacks with the imidazole ring of the axial ligand His63 in the offset π-stacking mode and with the porphyrin ring of heme in the T-stacking mode, as shown in Fig. 1 (Wu *et al.*, 2000; Durley & Mathews, 1996). In order to elucidate the contribution of the stacking interactions to the stability of cytochrome b_5, we have carried out site-directed mutagenesis at Phe58 of the trypsin-solubilized fragment of microsomal

cytochrome b_5 from bovine liver (Tb5) and the protein stability of the F58Y and F58W mutants has been studied and compared with that of the wild-type protein (WT-Tb5; Wu *et al.*, 2000). In this paper, we present the crystal structures of these two mutants. The structure of the F58Y mutant is basically the same as that of the wild-type protein; however, the mutation from Phe58 to Trp58 gives rise to multiple conformations and weakens the stacking interactions. The effect of the stacking interactions on the protein stability is discussed.

2. Materials and methods

2.1. Preparation of the mutant proteins

The F58Y and F58W genes were constructed according to the method described by Sambrook *et al.* (1989). The pUC19 plasmid containing the genes was transformed into *Escherichia coli* JM83 cells. The expression and purification of the F58Y and F58W mutant proteins were carried out by the same method as used for other mutants of cytochrome b_5 (Sun *et al.*, 1996), followed by lyophilization. The molecular weight was checked by electrospray ionization mass spectroscopy.

2.2. Crystallization

The F58Y and F58W proteins were crystallized using the hanging-drop vapour-diffusion method at 293 K under the following conditions: 3 µl protein solution at a concentration of 10 mg ml^{-1} was mixed with 3 µl reservoir solution containing 2.9–3.0 *M* phosphate buffer (pH 7.5–7.6). These conditions were similar to those used to crystallize the wild-type protein (WT-Tb5) and other mutants (Wu *et al.*, 2000). The reservoir solution used for F58W additionally contained dioxane at a concentration of 1%. F58Y crystals grew to dimensions of larger than $0.4 \times 0.4 \times 0.3$ mm within one week. However, it was much more difficult to grow single crystals of F58W, which usually gave twinned crystals or crystals with very weak diffraction. Only two usable single crystals, with dimensions of $0.3 \times 0.3 \times 0.25$ mm, grew from one droplet within one month.

2.3. X-ray data collection

One data set for F58Y and two data sets (set 1 and set 2) for F58W were collected at 293 K. Each data set was collected using a single crystal sealed in an X-ray capillary using a laboratory X-ray source and a CCD detector system. The X-ray data were collected to 1.70 and 2.32 Å resolution for F58Y and F58W, respectively. In order to collect data at high resolution for F58W, many crystals were frozen with 15–20% glycerol or sealed in X-ray capillaries and tested using synchrotron radiation, but none of them diffracted well. The F58W crystal that was already sealed in the X-ray capillary and had been used to collect data set 2 was then used to collect the third data set to 1.90 Å resolution using a CCD detector and synchrotron radiation at the Photon Factory, High Energy Accelerator Research Organization, Japan. All data were processed using *HKL*2000 software (Otwinowski & Minor,

Table 1
Crystal data and X-ray data-collection statistics.

Values in parentheses correspond to the data in the highest resolution shell (1.76–1.70 Å for F58Y and 2.49–2.40, 2.40–2.32 and 1.97–1.90 Å for data sets 1, 2 and 3 of F58W, respectively).

		F58W		
	F58Y†	Data set 1†	Data set 2†	Data set 3‡
Space group	C2	$P2_12_12_1$	$P2_12_12_1$	$P2_12_12_1$
Unit-cell parameters				
a (Å)	70.515	47.133	47.057	47.044
b (Å)	40.405	87.545	87.475	87.484
c (Å)	39.300	138.547	138.258	138.383
β (°)	111.699			
No. of molecules per AU	1	6	6	6
V_M§ (Å^3 Da^{-1})	2.58	2.35	2.34	2.34
Wavelength (Å)	1.5418	1.5418	1.5418	0.9789
Resolution (Å)	1.70	2.40	2.32	1.90
No. of unique reflections	9307	21053	25397	45329
R_{merge}¶ (%)	9.3 (34.2)	10.6 (42.5)	9.4 (52.4)	9.5 (57.1)
Data completeness (%)	87.6 (46.0)	90.6 (87.1)	99.9 (99.7)	98.8 (99.7)
Reflections with $I > 3\sigma(I)$ (%)	76.9 (67.0)	72.5 (45.6)	61.9 (26.3)	81.6 (49.9)

† Data were collected on an Apex CCD detector system equipped with D8 Discover X-ray generator with Cu target tube. ‡ Data were collected using synchrotron radiation with an CCD system at the Photon Factory, High Energy Accelerator Research Organization, Japan. § The volume per unit protein molecular weight (Matthews, 1968). ¶ $R_{merge} = \sum |I_i - \langle I_h \rangle| / \sum I_i$, where I_i is the ith observation of the intensity of the reflection h and $\langle I_h \rangle$ is the mean intensity for the reflection h from multiple measurements.

1997). The crystal data and data-collection statistics are listed in Table 1.

2.4. Structure determination

The crystal structure of F58Y was determined using the difference Fourier method based on the structure of WT-Tb5 at 1.9 Å resolution (Wu *et al.*, 2000), from which the side chain of Phe58 and all solvent molecules were omitted.

The crystal structure of F58W was determined using the molecular-replacement method. The most reasonable value of V_M (Matthews, 1968) for the F58W crystals corresponds to six molecules in an asymmetric unit; four or eight molecules would give marginal V_M values. The molecular-replacement procedure was unusually complicated as there were so many molecules in the asymmetric unit. The detailed procedure was as follows.

The self-rotation function was computed using the program *POLARRFN* from the *CCP*4 suite (Collaborative Computational Project, Number 4, 1994) to search for non-crystallographic symmetry. X-ray data (set 1) in the resolution range 8–5 Å were used and the integration radius was set to 20 Å, giving a predominant peak at $\varphi = 0$, $\psi = 43.5$, $\kappa = 180.0°$, as shown in Fig. 2, indicating a non-crystallographic twofold axis. This suggested that the following molecular-replacement strategy might simplify the molecular-replacement procedure: using one molecule as a search model to search for three molecules first and then taking these three molecules together as a search model to search for all six molecules.

Molecular replacement was carried out using the program *AMoRe* (Navaza, 1994) from the *CCP*4 suite. The molecular
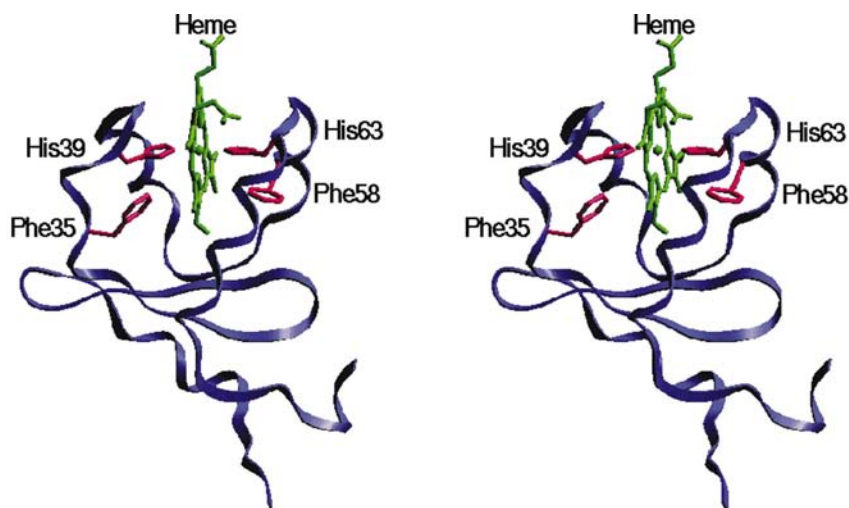
Figure 1
The ribbon diagram of WT-Tb5. The side chains of His39, His63, Phe35 and Phe58 are shown in red and heme is shown in green. This diagram was prepared using the molecular-graphics program *SETOR* (Evans, 1993).
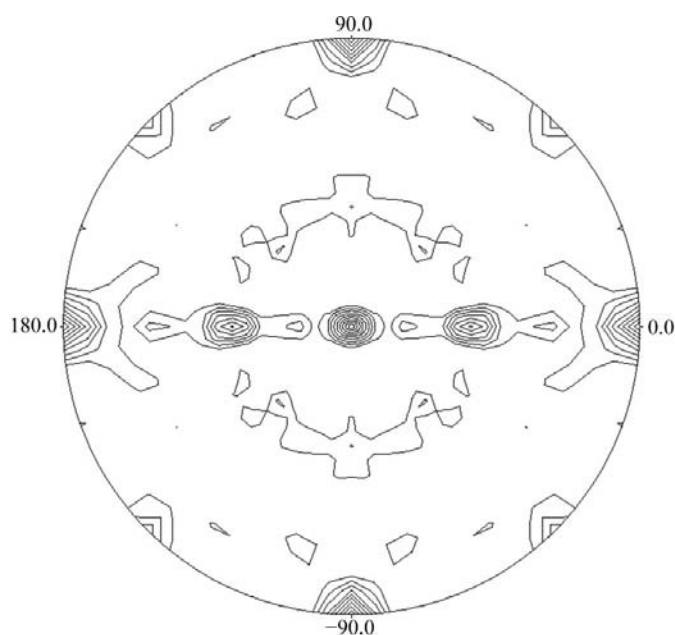
Figure 2
Self-rotation function of F58W at the $\kappa = 180.0°$ section. φ is proportional to the radius, from $0°$ (at the centre) to $90°$, and φ is labelled on the circle.

structure of WT-Tb5 (Wu *et al.*, 2000) was used as a search model; all the water molecules were omitted and Phe58 was replaced by alanine. X-ray data (set 1) in the resolution range 10–4 Å were used for calculation of the cross-rotation function and translation function as well as for rigid-body refinement.

The cross-rotation function gave two predominant peaks (Table 2*a*), one of which (No. 2) gave the highest CC_F value of the translation function (Table 2*b*), which was named solution *A*. This solution was then fixed and the above two rotation peaks were used to search for further translation-function peaks. The peak with the highest CC_F value from the translation function was taken as the second solution and

named *B* (Table 2*c*). The Eulerian angles were the same for these two solutions, suggesting that the two corresponding molecules have the same orientations. When solutions *A* and *B* were fixed and the above two rotation peaks were used again to search for more translation-function peaks, the five peaks (Table 2*d*) with highest CC_F values were taken one by one as the third solution to combine with solutions *A* and *B*. This group was then taken as a three-molecule search model. The three-molecule search succeeded only when the peak with the fifth highest CC_F value (Table 2*d*) was taken as the third solution, which was named solution *C*; in the other cases there were overlaps between the molecules. The three-molecule search model was composed of solutions *A* and *C* and the symmetry-related molecule of solution *B* (the symmetry operation brought *B* into proximity with *A* and *C*). The cross-rotation function using the three-molecule search model gave a total of three peaks and the first two gave much higher CC_F values than the third one (Table 2*e*). These two peaks gave high CC_F values of the translation function, which were named solutions *ABC* (Table 2*f*) and $D'E'F'$ (Table 2*g*), respectively.

Ten cycles of rigid-body refinement were applied to the solutions *ABC* and $D'E'F'$, giving CC_F and RF_F of 65.6 and 40.0, respectively, as shown in Table 2(*h*).

After the final solutions were applied to the three-molecule search model, the second group of the three molecules, $D'E'F'$, was then brought to the proximity of the first group *ABC* by the symmetry operator $(x - \frac{1}{2}, -y + \frac{1}{2}, -z + 1)$, giving molecules *DEF*. The molecules *ABCDEF* constituted the initial six-molecule model of F58W used for crystallographic refinement.

This model led to reasonable crystal packing in the unit cell and gave an *R* factor of 37.4% using the program *CNS* (Brünger *et al.*, 1998) with data set 1 in the resolution range 30–3 Å. When the $(F_o - F_c)$ difference electron-density map was computed based on the six-molecule model from which the iron ions had been omitted, it showed strongly positive peaks for iron at a contour level of 5–8σ. All these results suggested that the six-molecule model of F58W from molecular replacement should be correct.

2.5. Crystallographic refinement

Crystallographic refinement was carried out for F58Y and F58W mutants using *CNS* (Brünger *et al.*, 1998). 10% of the data were randomly excluded from the refinement and used as a test data set to monitor R_{free} (Brünger, 1992). The model fitting was carried out with the graphics software *TURBO-FRODO* (Roussel & Cambillau, 1991).

After one round of simulated-annealing refinement and temperature-factor refinement of F58Y at 2.2 Å resolution, the $(2F_o - F_c)$ and $(F_o - F_c)$ electron-density maps were

Table 2
Molecular-replacement solutions.

(a) Cross rotation-function solutions using one-molecule search model (integration radius 21 Å). α, β, γ are the Eulerian angles. CC_F is the correlation coefficient between the observed amplitudes for the crystal and the calculated amplitudes for the model. The CC_F value of the third peak was 4.3. RF_F is the classic R factor (%) between the observed amplitudes for the crystal and the calculated amplitudes for the model.

Peak No.	α (°)	β (°)	γ (°)	CC_F	RF_F
1	129.65	57.22	260.38	6.6	58.9
2	54.46	54.54	6.50	6.9	58.8

(b) Translation-function solutions using one-molecule search model. T_x, T_y, T_z are translation vectors (fractional).

Peak No.	α (°)	β (°)	γ (°)	T_x	T_y	T_z	CC_F	RF_F
1	129.65	57.22	260.38	0.2694	0.4511	0.4438	12.7	58.5
2→A	54.46	54.54	6.50	0.0907	0.2010	0.0201	16.2	57.1

(c) Translation-function solutions using one-molecule search model.

Peak No.	α (°)	β (°)	γ (°)	T_x	T_y	T_z	CC_F	RF_F
A fixed	54.46	54.54	6.50	0.0907	0.2010	0.0201		
1	129.65	57.22	260.38	0.1632	0.4509	0.4424	25.0	55.6
1	129.65	57.22	260.38	0.2687	0.4489	0.1032	22.6	56.4
2→B	54.46	54.54	6.50	0.9846	0.2016	0.6822	35.0	53.5

(d) Translation-function solutions using one-molecule search model.

Peak No.	α (°)	β (°)	γ (°)	T_x	T_y	T_z	CC_F	RF_F
A fixed	54.46	54.54	6.50	0.0907	0.2010	0.0201		
B fixed	54.46	54.54	6.50	0.9846	0.2016	0.6822		
1	129.65	57.22	260.38	0.1628	0.4502	0.4425	39.1	51.1
1	129.65	57.22	260.38	0.2734	0.4491	0.7819	36.4	52.1
1→C	129.65	57.22	260.38	0.2701	0.4489	0.1042	35.8	52.3
2	54.46	54.54	6.50	0.9840	0.2022	0.3604	45.0	52.8
2	54.46	54.54	6.50	0.0922	0.2013	0.3430	43.0	53.1

(e) Cross rotation-function solutions using three-molecule search model (integration radius 28 Å). The three-molecule search model is composed of solutions A and C and the symmetry-related molecule of solution B (symmetry operator: $\frac{1}{2} - x + 1$, $-y + 1$, $z - \frac{1}{2}$). The CC_F value of the third peak is 8.7.

Peak No.	α (°)	β (°)	γ (°)	CC_F	RF_F
1	19.00	84.10	111.57	13.9	57.2
2	82.44	19.85	30.46	12.7	57.6

(f) Translation-function solutions using three-molecule search model. The CC_F value of the third peak is 20.2.

Peak No.	α (°)	β (°)	γ (°)	T_x	T_y	T_z	CC_F	RF_F
1→ABC	19.00	84.10	111.57	0.2927	0.0173	0.0590	38.8	51.1
2	82.44	19.85	30.46	0.0846	0.2659	0.3287	26.4	55.2

(g) Translation-function solutions using three-molecule search model.

Peak No.	α (°)	β (°)	γ (°)	T_x	T_y	T_z	CC_F	RF_F
ABC fixed	19.00	84.10	111.57	0.2927	0.0173	0.0590		
2→D′E′F′	82.44	19.85	30.46	0.0863	0.2662	0.8283	63.3	41.5

(h) Rigid-body refinement.

Peak No.	α (°)	β (°)	γ (°)	T_x	T_y	T_z	CC_F	RF_F
ABC	19.14	83.62	112.14	0.2923	0.0161	0.0593	66	40.0
D′E′F′	86.78	19.61	26.68	0.0858	0.2671	0.8278		

computed and the side chain of Tyr58 was built. The structure was further refined and the X-ray data used for refinement were gradually extended to 1.86 Å resolution. Water molecules were included in the model when the structure was refined to 2.0 Å resolution and only water molecules with $B < 50$ Å^2 were included in the final model.

The F58W structure was first refined using data set 1, starting from 3.0 Å resolution, and the $(2F_o - F_c)$ and $(F_o - F_c)$ electron-density maps were computed after one round of simulated-annealing refinement followed by temperature-factor refinement. The maps showed large pieces of electron density at the side chain of the 58th residue. Fitting of the Trp58 side chain was carried out followed by further refinement and the resolution was gradually extended. The non-crystallographic symmetry was not imposed because it would produce poor electron density in some regions, which can be attributed to the multiple conformations in this structure (see below). Data set 2 was then collected and used to further refine the structure. After the synchrotron data had been collected, they were used to extend the refinement to 2.0 Å resolution. Manual rebuilding was performed from time to time during the refinement using $(2F_o - F_c)$ and $(F_o - F_c)$ maps; simulated-annealing 'omit' maps (Hodel *et al.*, 1992) were computed for some questionable residues. Water molecules were included in the model and in the last stage the multiple conformations were built for some residues and the structure was further refined.

3. Results

3.1. Quality of the crystal structures

The crystal structures of the F58Y and F58W mutants were refined at 1.86 and 2.0 Å, respectively. The crystallographic refinement statistics are shown in Table 3. The R factors of the F58Y and F58W structures are 19.0 and 22.4%, respectively, and R_{free} is 21.5 and 26.6%, respectively. Four residues of F58W fall into the disallowed region of the Ramanchandran plot: His26 of molecules *A*, *B*, *D* and *F* (see below).

Table 3
Refinement statistics.

Values in parentheses correspond to data in the highest resolution shell (1.93–1.86 Å for F58Y and 2.07–2.00 Å for F58W). The data in higher resolution shells were not used for refinement owing to the low completeness or high R_{merge} of the data.

	F58Y	F58W
Resolution (Å)	1.86	2.0
No. of amino-acid residues	82	492
No. of prosthetic groups	1	6
No. of solvent molecules	67	150
R factor† (%)	19.0 (25.3)	22.4 (26.9)
Free R factor‡ (%)	21.5 (26.6)	26.6 (31.4)
R.m.s.d.§		
Bond lengths (Å)	0.0106	0.0091
Bond angles (°)	1.1	1.2
Dihedrals (°)	22.5	23.16
Impropers (°)	0.95	0.94
Mean temperature factors (Å²)		
Main chain	19	31
Side chain	23	35
Heme	21	25
Solvent	38	39
Residues in Ramachandran plot¶ (%)		
Most favoured region	90.3	91.9
Additional allowed region	9.7	6.9
Generously allowed region	0.0	0.2
Mean atomic coordinate error†† (Å)	0.22	0.26

† $R = \sum ||F_o| - |F_c|| / \sum |F_o|$. ‡ R_{free} was calculated from 10% of the X-ray data randomly selected for cross-validation (Brünger, 1992) § Root-mean-square deviation. ¶ Calculated using *PROCHECK* (Morris *et al.*, 1992). †† Obtained from Luzzati plot (Luzzati, 1952).

Table 4
R.m.s. deviations of C$^\alpha$ atoms between the six molecules of F58W as well as between WT-Tb5 and each F58W molecule.

	A	B	C	D	E	F	WT-Tb5
A		0.16	0.52	0.15	0.46	0.31	0.55
B			0.48	0.19	0.41	0.27	0.51
C				0.53	0.28	0.35	0.63
D					0.47	0.33	0.53
E						0.24	0.56
F							0.51

3.2. Crystal structure of F58Y

The space group, unit-cell parameters (Table 1) and the overall crystal structure of F58Y are the same as those of WT-Tb5 (Wu *et al.*, 2000). The local structure around the mutation site, including the conformation of the phenol ring of Tyr58, is also very similar to that of WT-Tb5 and the hydroxyl group of Tyr58 enters the solvent area and forms a hydrogen bond with a water molecule. This water molecule also exists in WT-Tb5 and is hydrogen bonded to the side chain of Ser71, while in the F58Y structure it has moved by 0.5 Å and is hydrogen bonded to both Tyr58 and Ser71; meanwhile, the C$^\beta$—C$^\gamma$ bond of Tyr58 is rotated by approximately 2° to bring its hydroxyl group closer to this water molecule.

3.3. Crystal structure of F58W

The mutation from Phe58 to Trp58 results in a space-group change from $C2$ to $P2_12_12_1$; there are six molecules in the asymmetric unit. The unit-cell parameters of the F58W mutant are listed in Table 1.

The self-rotation function (Lattman, 1985) revealed a predominant peak at $\varphi = 0$, $\psi = 43.5$, $\kappa = 180°$ (Fig. 2), indicating a non-crystallographic twofold axis.

Fig. 3 shows the six molecules in the asymmetric unit. *ABC* and *DEF* are related by a non-crystallographic twofold axis, which agrees with the result from the self-rotation function. The r.m.s. difference between *ABC* and *DEF* is 0.47 Å. The matrix and translation vector to transform molecules *ABC* to *DEF* are

$$\text{matrix} = \begin{pmatrix} 0.13223 & 0.01777 & -0.99106 \\ -0.00909 & -0.99978 & -0.01914 \\ -0.99118 & 0.01154 & -0.13204 \end{pmatrix},$$

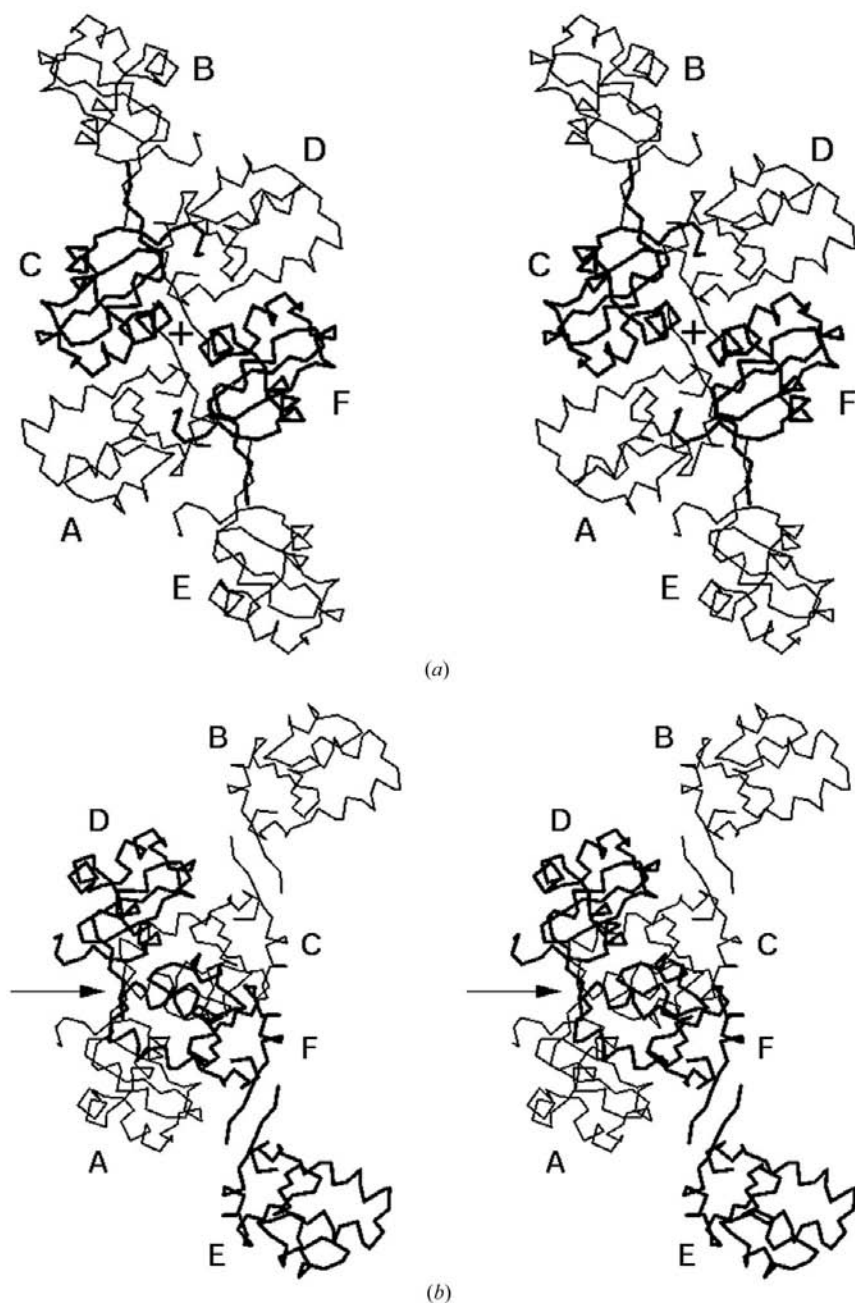$$\text{translation vector} = (\, 33.82729 \quad 22.08765 \quad 38.66743 \,).$$

The secondary structure of the F58W mutant does not change because of the mutation except that there are three pairs of intermolecular (*A–D, B–C, E–F*) two-stranded antiparallel β-sheets composed of the N-terminal segments, each β-sheet containing a pair of hydrogen bonds between Val4–Tyr6 of the pair of molecules, as shown in Fig. 3(*b*). The tertiary structure of F58W is also similar to that of WT-Tb5 and Table 4 lists the r.m.s. deviations of the C$^\alpha$ atoms between the six molecules as well as those between WT-Tb5 and each F58W molecule.

Obvious changes in the tertiary structure of F58W compared with WT-Tb5 were observed in the segments Asn16–Ser20, His26–Tyr27 and Val61–Ser64 in addition to the N- and C-terminal segments. The difference in His26–Tyr27 between F58W and WT-Tb5 will be described below. Asn16–Ser20 is a flexible segment (Wu *et al.*, 2000, 2002) and is involved in intermolecular interactions in WT-Tb5 (Wu *et al.*, 2000) but not in F58W. For example, the deviations of the C$^\alpha$ atoms of Ser18 in the six molecules of F58W from those of WT-Tb5 are in the range 2.4–3.2 Å. The difference in the local structure of the loop segment Val61–Ser64 of F58W from WT-Tb5 results from introducing the large side chain of Trp58 nearby. In addition, the main-chain conformations of this segment differ slightly from one another among the six molecules of F58W. For example, there is a hydrogen bond between Asp57 O and Val61 N in WT-Tb5 which is maintained in molecules *A*, *B* and *D*, but the distances between these two atoms are increased to 3.7–3.8 Å in molecules *C*, *E* and *F*, and the main-chain O atoms of Asp60 are involved in intermolecular hydrogen bonds in all six molecules of F58W but not in WT-Tb5. The axial ligand His63 is located in this segment and the deviations of the C$^\alpha$ atoms of His63 in the six molecules from those of WT-Tb5 are larger than 0.6 Å. However, the conformations and orientations of the imidazole rings of His63 in the six molecules are still similar to each other and to that of WT-Tb5, with the ring atoms deviating by less than 0.4 Å.

The conformations of the mutation-site residues Trp58 in the six molecules are similar to each other. The C$^\gamma$ atoms deviate from each other by less than 0.15 Å when they are superimposed. Compared with WT-Tb5, the deviations of C$^\alpha$ and C$^\gamma$ atoms are approximately 0.3 and 0.6 Å, respectively. The angles between the indole ring of Trp58 and the imidazole ring of His63, and between the Trp58 indole ring and the mean plane of the heme ring, when compared with the phenyl ring of WT-Tb5, are increased and decreased, respectively, by

(a)

(b)

Figure 3
The six molecules of F58W in an asymmetric unit. (a) This diagram is viewed along the non-crystallographic twofold axis, which is shown as a cross. Molecules C and F are shown in thick lines and the other four molecules in thin lines. (b) This diagram is rotated by 90° from Fig. 3(a). The non-crystallographic twofold axis is shown as an arrow. Molecules A, B and C are shown in thin lines and D, E and F in thick lines. These diagrams were prepared using the molecular-graphics program SETOR.

approximately 10°. Fig. 4(a) shows the electron density of the side chains of Trp58 and His63 as well as the heme in F58W in molecule A as an example. Figs. 4(b) and 4(c) show the conformations of Trp58, His63 and heme of F58W (in molecule A) superimposed with the corresponding residues of WT-Tb5.

The mutation from Phe58 to Trp58 gives rise to multiple conformations of Glu59, the neighbouring residue of Phe/Trp58. In the WT-Tb5 structure, the side chain of Glu59 forms salt-bridge and hydrogen-bond interactions with Arg68 and His26 of the same molecule (Fig. 5a) and does not interact with the symmetry-related molecules. The mutation from Phe58 to Trp58 introduces a larger side chain into the heme-binding pocket, which is in the neighbourhood of Glu59. In the F58W structure the side chains of Glu59 form intermolecular hydrogen bonds in all six molecules, i.e. in molecules A, B and D they interact with the hydroxyl group of Tyr7 of other molecules and in molecules C and E with the main-chain N atom of Ala3 of other molecules. The side chains of Glu59 keep conformations similar to those of WT-Tb5 in molecules C and E, with intramolecular interactions of Glu59 with Arg68 and His26 being maintained in these two molecules; the conformations of Arg68 and His26 in molecules C and E are also similar to those in WT-Tb5 except for the guanidino groups of the side chains of Arg68. However, the conformations of Glu59 differ from those of WT-Tb5 in molecules A, B and D, which in turn leads to the conformational changes of the side chains of Arg68 and His26 in these three molecules; Arg68 in molecules A, B and D forms an intermolecular salt bridge with Glu10 of another molecule instead of an intramolecular salt bridge with Glu59. In molecules A, B and D the changes in the His26 side chains are accompanied by conformational changes of the side chains of the neighbouring residue Tyr27 and the peptide bonds linking His26 and Tyr27 are flipped by 180°. However, the changes in His26–Tyr27 do not occur in molecules C and E compared with WT-Tb5. In molecule F these four residues, Glu59, Arg68, His26 and Tyr27, exhibit dual conformations, one similar to those in molecules A, B and D and the other similar to those in C and E, each conformation having an occupancy of approximately 0.5. The flipping of the peptide linking His26 and Tyr27 in molecules A, B and D and one of the conformations of F results in the unusual

conformational angles of the main chain, which fall into the disallowed region of the Ramachandran plot. The conformations of these four residues in molecules A, C and F are shown in Figs. 5(b) and 5(c). Fig. 6 shows the electron density of His26 and Tyr27 in molecule F.
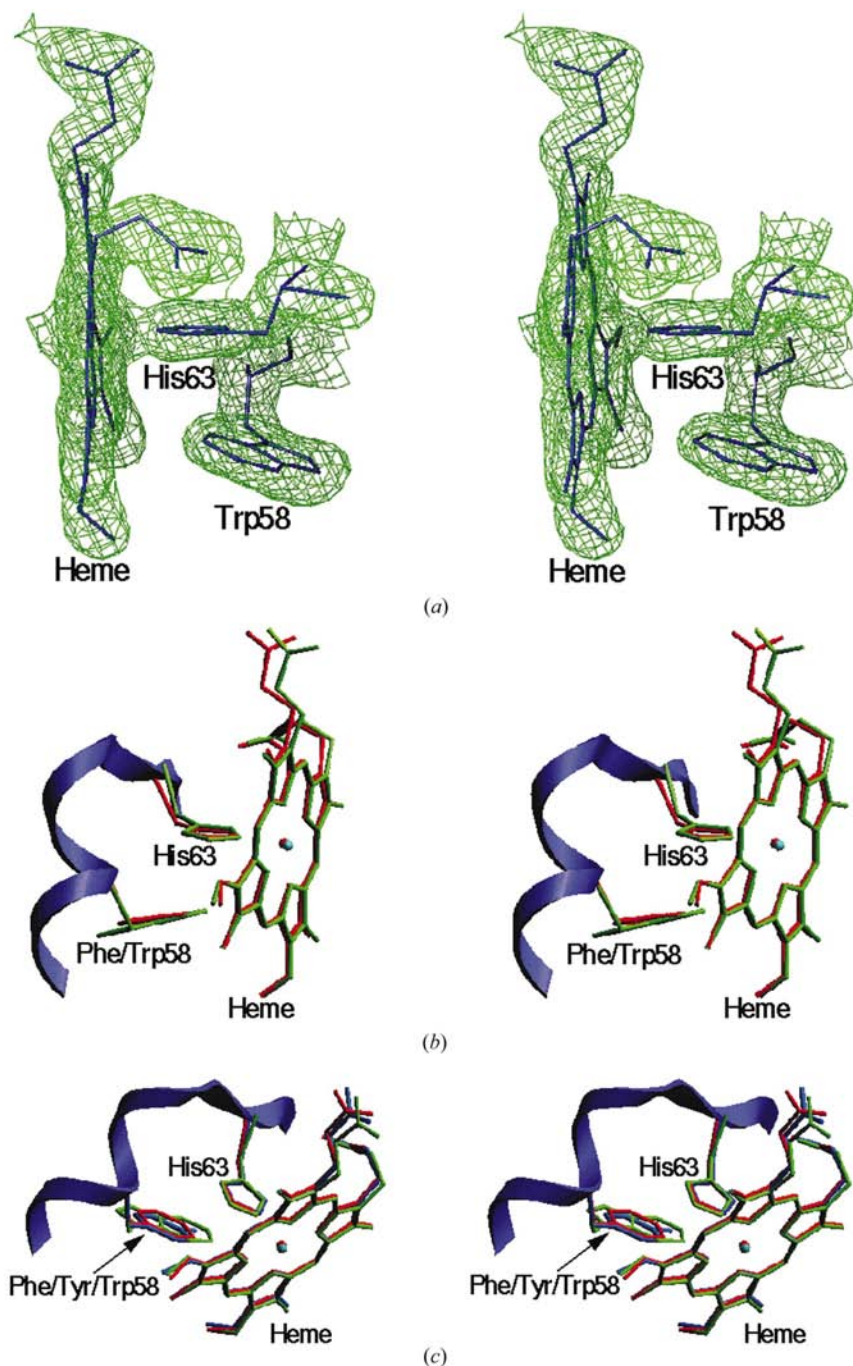
In addition, residues Lys28 and Lys72 also exhibit multiple conformations in the F58W mutant, as shown in Figs. 5(b) and

5(c). In WT-Tb5 one of the propionic acids of the heme is hydrogen bonded to Ser64 (Wu $et\ al.$, 2000; Durley & Mathews, 1996) and its conformation is conserved in all the mutants of Tb5 (Xue $et\ al.$, 1999; Gan $et\ al.$, 2002; Wu $et\ al.$, 2002; Wang, Wu $et\ al.$, 2002; Yao $et\ al.$, 2002), including F58Y; however, the other propionic acid group is extended into the solvent and is more flexible. The extended groups also exhibit multiple conformations in the F58W mutant (Figs. 5b and 5c). In WT-Tb5, Lys72 and the extended propionic acid group of the heme do not interact with other molecules and Lys28 is involved in intermolecular interactions. In F58W the extended propionic acid groups of hemes in molecules A, B and D form intermolecular salt bridges with Lys72 and those in molecules C, E and F with Lys28. The different intermolecular interactions result in conformational differences in residues Lys28 and Lys72 and the extended propionic acid groups of hemes between the two groups of the molecules: the conformations of these in molecules A, B and D are similar to those in WT-Tb5, while those in molecules C, E and F differ from those of WT-Tb5. In addition, the heme porphyrin rings of C, E and F make a small rotation (approximately 5°) within the mean plane compared with that of WT-Tb5, while those of molecules A, B and D are oriented more similarly to that of WT-Tb5.

In summary, the six molecules of F58W can be grouped into two types: A, B and D, and C, E and F. The conformations of the side chains of Glu59, Arg68, His26 and Tyr27 as well as the peptide bond linking His26 and Tyr27 are different from those of WT-Tb5 for the first group and are similar to those of WT-Tb5 for the second group, with the exception of molecule F, in which they exhibit dual conformations. The side chains of Lys28, Lys72 and the extended propionic acid groups of the hemes show conformations that are similar to those in WT-Tb5 for the first group and different from those of WT-Tb5 for the second group. These multiple conformations can be primarily attributed to the mutation from Phe58 to a larger Trp58 in the neighbourhood of Glu59; the different intermolecular interactions between the two groups also contribute to the differences.
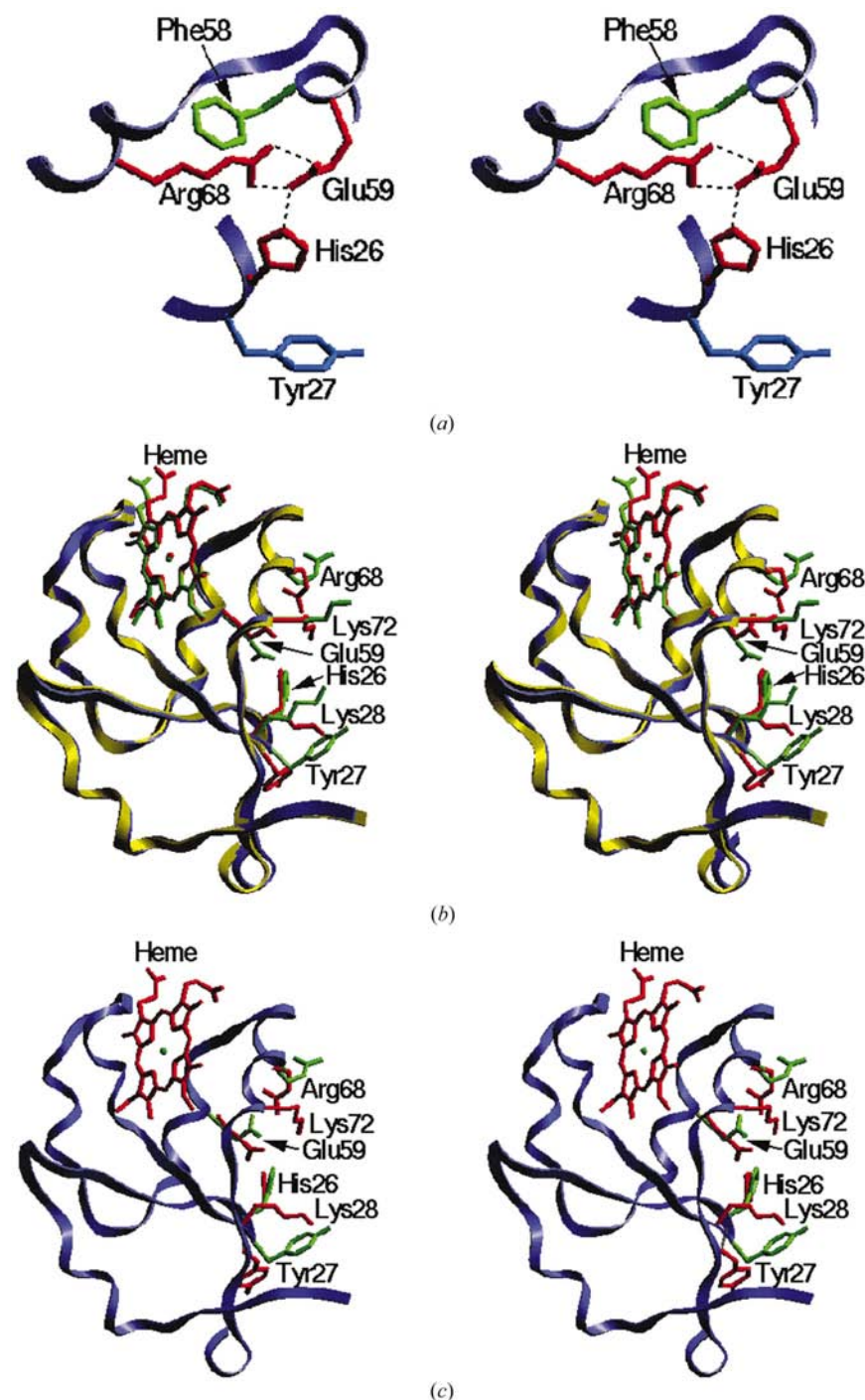

Figure 4
Trp58, His63 and heme of F58W (molecule A). (a) ($2F_o - F_c$) electron density of the side chains of Trp58 and His63 as well as heme, contoured at 1.2σ. This diagram was prepared using the molecular-graphics program $TURBO$-$FRODO$. (b) Trp58, His63 and heme of F58W shown in green, superimposed with the corresponding residues of WT-Tb5 shown in red. (c) The same as (b) except in a different view; Tyr58 in F58Y is also superimposed and shown in blue. (b) and (c) were prepared using the molecular-graphics program $SETOR$.

4. Discussion

WT-Tb5 and its other mutants yielded good crystals which diffracted to 1.8–2.1 Å reso-

lution and the refined structures gave *R* factors of around 19% (Xue *et al.*, 1999; Wu *et al.*, 2000, 2002; Gan *et al.*, 2002; Wang, Wu *et al.*, 2002; Yao *et al.*, 2002), including the F58Y mutant

presented in this paper. However, it was exceedingly difficult to grow single crystals of the F58W mutant. For this mutant dioxane was helpful and only two single crystals grew in one droplet. The structure of the F58W mutant contains six molecules in an asymmetric unit accompanying the space-group change and the structure shows some unusual features: six side chains and one of the propionic acid groups of the heme exhibit two types of conformations in the six molecules. Furthermore, four of the six side chains and the peptide bond linking two of the six residues show dual conformations in one of the six molecules. These results suggest that the multiple conformations exist in the protein solution before crystallization and the protein can crystallize as single crystals only when the ratio of the different conformations in the solution is appropriate. For example, the two conformations of Glu59, Arg68, His26 and Tyr27 have to be in the ratio 3.5:2.5 in order to grow the crystal form presented in this paper. This condition is difficult to attain, which accounts for the difficulty in growing single crystals of the F58W mutant. Therefore, it is suggested that the problems with the crystallization of the F58W mutant resulted from the multiple conformations of a few residues near the mutation site. Even if single crystals are grown, the crystal form changes compared with the wild-type protein and the crystals are less perfect, leading to lower resolution of the diffraction data and the higher *R* factor for the refined structure.

The F58W mutant structure contains six molecules in the asymmetric unit, which leads to the complexity of the molecular replacement. The structure determination succeeded by making use of the non-crystallographic symmetry, as described in §2. The rotation-function solutions *A* and *B* gave the same rotation angles (Table 2*c*), indicating that the two sets of molecules are oriented similarly to each other, so that the correct translation solutions can be found only when this rotation solution was repeatedly used.

Table 4 shows the r.m.s. deviations between the six molecules of F58W as well as between each of them and WT-Tb5. Molecule *C* exhibits the largest r.m.s. deviation from WT-Tb5 (0.63 Å) and the r.m.s. deviations between WT-Tb5 and each of the other five molecules are in the range 0.51–0.55 Å. As described above, the six

Figure 5
Multiple conformations of F58W. (*a*) The salt bridge and hydrogen-bonding interactions of Glu59 with Arg68 and His26 in WT-Tb5. Glu59, Arg68 and His26 are shown in red. The salt bridge and hydrogen bonds are shown in dashed lines. Phe58 and Tyr27 are shown in green and blue, respectively. (*b*) The superimposed Cα backbones of molecules *A* and *C* of F58W are shown as blue and yellow ribbons, respectively. The side chains of His26, Tyr27, Lys28, Glu59, Arg68, Lys72 and heme are shown in green and red for molecules *A* and *C*, respectively. (*c*) The Cα backbone of molecule *F* is shown as a blue ribbon. The side chains of Lys28, Lys72 and heme are shown in red. The two conformations of the side chains of His26, Tyr27, Glu59 and Arg68 are shown in red and green, respectively.

molecules can be grouped into two types: *A*, *B* and *D*, and *C*, *E* and *F*. As shown in Table 4, the r.m.s. deviations between the molecules within the same group are smaller: less than 0.2 Å within the first group and around 0.3 Å within the second group. Molecule *F* gives moderate r.m.s. deviations of around 0.3 Å from any of the other five molecules. Larger deviations of greater than 0.4 Å appear between the two groups.

A kinetic study of the heme-transfer reaction between cytochrome b_5 and apo-myoglobin exhibited a striking increase in the rate constant for the F58W mutant and a slight increase for the F58Y mutant (k = 1.30, 1.51 and 5.51 h^{-1} for WT-Tb5, F58Y and F58W, respectively; Wang, Lu *et al.*, 2002), which suggested that the mutation from Phe58 to Trp58 leads to markedly easier dissociation of the heme prosthetic group in F58W than in WT-Tb5 and that there is only a slight influence in the F58Y mutant. This is mainly attributed to the increase and decrease by 5–10° of the angles between the indole ring of Trp58 and the imidazole ring of His63 and between the Trp58 indole ring and the heme ring, respectively, in the F58W mutant compared with in WT-Tb5, which weakens the stacking interactions and enables the heme to leave more easily in F58W than in WT-Tb5. In the F58Y mutant structure, the stacking interactions are slightly weakened owing to a conformational change of only 2° of the side chain of Tyr58 compared with Phe58 of WT-Tb5. A thermal denaturation study and a guanidine hydrochloride-mediated unfolding procedure monitored by UV–visible and fluorescence spectra also indicated that the protein stability is decreased for both the F58Y and F58W mutants compared with WT-Tb5 and that F58W is less stable than F58Y: the midpoint
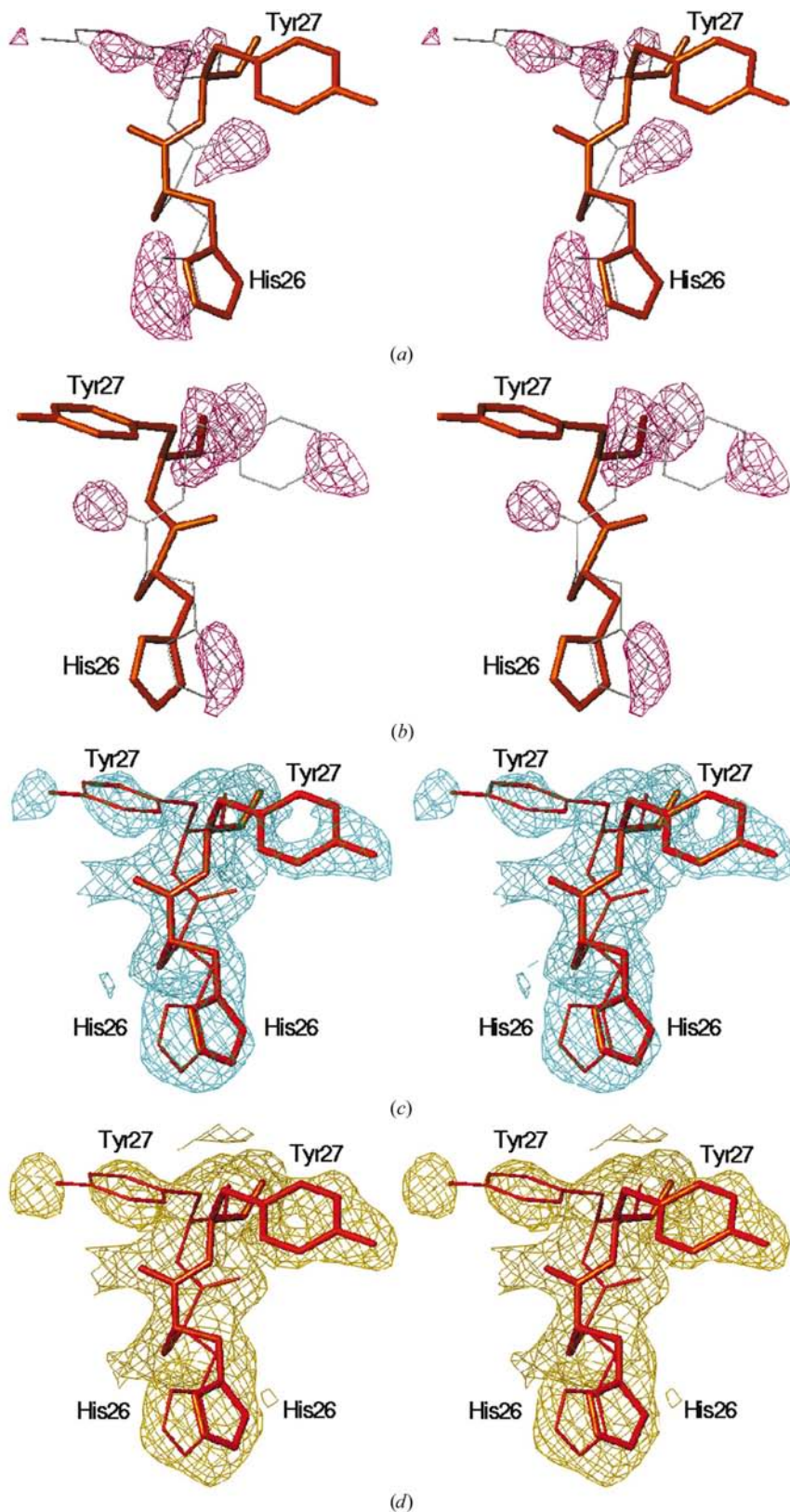
Figure 6
The electron density of the side chains of His26 and Tyr27 as well as the peptide bond linking them in molecule *F* of F58W. (*a*) The ($F_o − F_c$) difference electron density when the structure contains the first conformation only (thick red lines) contoured at +3.0σ. The second conformation was absent in the model and is shown in thin grey lines. (*b*) The ($F_o − F_c$) difference electron density when the structure contains the second conformation only (thick red lines) contoured at +3.0σ. The first conformation was absent in the model and is shown in thin grey lines. (*c*) The ($2F_o − F_c$) electron density contoured at 0.8σ for the final structure model containing dual conformations of the side chains of His26 and Tyr27 as well as the peptide linking His26 and Tyr27. The two conformations are shown in thin and thick red lines. (*d*) The ($F_o − F_c$) simulated-annealing 'omit' electron density when His26 and Tyr27 were omitted from the map computation, contoured at +3.0σ. The final structure model is superimposed with the map and the two conformations are shown in thin and thick red lines.

temperatures were 340.5, 337.6 and 336.9 K, and the midpoint concentrations of guanidine hydrochloride were 2.89, 2.76 and 2.70 M for WT-Tb5, F58Y and F58W, respectively (Wang, Lu *et al.*, 2002).

The calculated potential energy of a dibenzene model system has been reported (Burley & Petsko, 1986), which showed that in some cases a change of $10°$ in the interplanar angle would influence the stacking energy dramatically. For example, an increase of $10°$ in the interplanar angle increases the energy by approximately 20 kJ mol^{-1} when the centroid–centroid separation r is 5 Å, the central–normal angle θ is $50°$ and the interplanar angle is around $20°$; a decrease of $10°$ in the interplanar angle increases the energy by approximately 15 kJ mol^{-1} when the centroid–centroid separation r is 5.5 Å, the central–normal angle θ is $50°$ and the interplanar angle is around $70°$. When molecule C of F58W is taken as an example, r is approximately 4.5 Å and the interplanar angle is approximately $20°$ for the stacking with His63, r is approximately 7 Å and the interplanar angle is approximately $70°$ for the stacking with heme, the θ values are approximately $40°$ in both cases and the interplanar angles are increased and decreased for the stacking with His63 and with heme, respectively, by approximately $10°$ owing to the mutation. These are similar to the above-mentioned conditions in the reference, which accounts for the striking increase of the rate constant of the heme-transfer reaction. The calculated stacking energy of the model system may not represent the exact energy in our system since the two systems are different, the F58W mutant being a protein and dibenzene a small molecule, with the aromatic groups being different in the two systems and the centroid–centroid separation of 7 Å for Trp58-heme stacking being beyond the range of r for the calculation of the model system. However, the data calculated from the model system suggest a trend of a dramatic change in the stacking energy resulting from a change of $10°$ in the interplanar angle of F58W, which leads to the great weakening of the stacking interactions and the easier removal of the heme from the pocket compared with WT-Tb5.

The stacking interactions have a lower effect on protein denaturation than on the heme-transfer reaction rates since the crystal structure shows that the secondary and tertiary structures of the protein do not change greatly.

In addition to the weakening of the stacking interactions, there may be other factors that could also slightly influence the protein stability, such as the introduction of an electronegative N atom on the indole ring of Trp58 into the heme-binding pocket; this might decrease the hydrophobicity of the pocket and permit the heme to leave more easily.

References

Brünger, A. T. (1992). *Nature (London)*, **335**, 472–475.
Brünger, A. T., Adams, P. D., Clore, G. M., DeLano, W. L., Gros, P., Gross-Kunstleve, R. W., Jiang, J.-S., Kuszewski, J., Nilges, N., Pannu, N. S., Read, R. J., Rice, L. M., Simonson, T. & Warren, G. L. (1998). *Acta Cryst.* D**54**, 905–921.
Burley, S. K. & Petsko, G. A. (1985). *Science*, **229**, 23–28.
Burley, S. K. & Petsko, G. A. (1986). *J. Am. Chem. Soc.* **108**, 7995–8001.
Collaborative Computational Project, Number 4 (1994). *Acta Cryst.* D**50**, 760–763.
Cowley, A. B., Altuve, A., Kuchment, O., Terzyan, S., Zhang, X. C., Rivera, M. & Benson, D. (2002). *Biochemistry*, **41**, 11566–11581.
Durley, R. C. E. & Mathews, F. S. (1996). *Acta Cryst.* D**52**, 65–76.
Evans, S. V. (1993). *J. Mol. Graph.* **11**, 134–138.
Funk, W. D., Lo, T. P., Mauk, M. R., Brayer, G. D., MacGillivray, R. T. A. & Mauk, A. G. (1990). *Biochemistry*, **29**, 5500–5508.
Gan, J.-H., Wu, J., Wang, Z.-Q., Wang, Y.-H., Huang, Z.-X. & Xia, Z.-X. (2002). *Acta Cryst.* D**58**, 1298–1306.
Hodel, A., Kim, S.-H. & Brünger, A. T. (1992). *Acta Cryst.* A**48**, 851–858.
Hunter, C. A. & Sanders, J. K. M. (1990). *J. Am. Chem. Soc.* **112**, 5525–5534.
Lattman, E. (1985). *Methods Enzymol.* **115**, 55–77.
Liu, D., Williamson, D. A., Kennedy, M. L. & Williams, T. D. (1999). *J. Am. Chem. Soc.* **121**, 11798–11812.
Luzzati, P. V. (1952). *Acta Cryst.* **5**, 802–810.
Matthews, B. W. (1968). *J. Mol. Biol.* **33**, 491–497.
Morris, A. L., MacArthur, M. W., Hutchinson, E. G. & Thornton, J. M. (1992). *Proteins Struct. Funct. Genet.* **12**, 345–364.
Navaza, J. (1994). *Acta Cryst.* A**50**, 157–163.
Otwinowski, Z. & Minor, W. (1997). *Methods Enzymol.* **276**, 307–326.
Ren, Y., Wang, W.-H., Wang, Y.-H., Case, M., Qian, W., McLendon, G. & Hung, Z.-X. (2004). *Biochemistry*, **43**, 3527–3536.
Rivera, M., Seetharaman, R., Girdhar, D., Wirtz, M., Zhang, X., Wang, X. & White, S. (1998). *Biochemistry*, **37**, 1485–1494.
Roussel, A. & Cambillau, C. (1991). *Silicon Graphics Partners Geometry Dictionary*. Silicon Graphics, Mountain View, CA, USA.
Sambrook, J., Fritsch, E. P. & Maniatis, T. (1989). *Molecular Cloning: A Laboratory Manual*, 2nd ed, pp. 201–233. Plainview: Cold Spring Harbor Laboratory Press.
Sun, Y.-L., Xie, Y., Wang, Y.-H., Xiao, G. T. & Huang, Z.-X. (1996). *Protein Eng.* **9**, 555–558.
Wang, Y.-H., Lu, J.-X., Wang, W.-H., Ren, Y., Xie, Y. & Huang, Z.-X. (2002). *Chin. Sci. Bull.* **47**, 1707–1710. In Chinese.
Wang, Z.-Q., Wu, J., Wang, Y.-H., Qian, W., Xie, Y., Xia, Z.-X. & Huang, Z.-X. (2002). *Chin. J. Chem.* **20**, 1212–1224.
Wu, J., Gan, J.-H., Xia, Z.-X., Wang, Y.-H., Wang, W.-H., Xue, L.-L., Xie, Y. & Huang, Z.-X. (2000). *Proteins Struct. Funct. Genet.* **40**, 249–257.
Wu, J., Wang, Y.-H., Gan, J.-H., Wang, W.-H., Sun, B.-Y., Huang, Z.-X. & Xia, Z.-X. (2002). *Chin. J. Chem.* **20**, 1225–1234.
Xue, L.-L., Wang, Y.-H., Xie, Y., Yao, P., Wang, W.-H., Qian, W., Huang, Z.-X., Wu, J. & Xia, Z.-X. (1999). *Biochemistry*, **38**, 11961–11972.
Yao, P., Wu, J., Wang, Y.-H., Sun, B.-Y., Xia, Z.-X. & Huang, Z.-X. (2002). *Eur. J. Biochem.* **269**, 4287–4296.